NANO LETTERS
Cite This: Nano Lett. 2018, 18, 3017−3023
Letter
pubs.acs.org/NanoLett

Reconfigurable Vanadium Dioxide Nanomembranes and Microtubes with Controllable Phase Transition Temperatures

Ziao Tian,[†,⊥] Borui Xu,[†,⊥] Bo Hsu,[‡] Liliana Stan,[§] Zheng Yang,[‡] and YongFeng Mei*[,†]

[†]Department of Materials Science, State Key Laboratory of ASIC and Systems, Fudan University, 200433 Shanghai, PR China
[‡]Department of Electrical and Computer Engineering, University of Illinois at Chicago, Chicago, Illinois 60607, United States
[§]Center for Nanoscale Materials, Argonne National Laboratory, Lemont, Illinois 60439, United States

Supporting Information

ABSTRACT: Two additional structural forms, free-standing nanomembranes and microtubes, are reported and added to the vanadium dioxide (VO_2) material family. Free-standing VO_2 nanomembranes were fabricated by precisely thinning as-grown VO_2 thin films and etching away the sacrificial layer underneath. VO_2 microtubes with a range of controllable diameters were rolled-up from the VO_2 nanomembranes. When a VO_2 nanomembrane is rolled-up into a microtubular structure, a significant compressive strain is generated and accommodated therein, which decreases the phase transition temperature of the VO_2 material. The magnitude of the compressive strain is determined by the curvature of the VO_2 microtube, which can be rationally and accurately designed by controlling the tube diameter during the rolling-up fabrication process. The VO_2 microtube rolling-up process presents a novel way to controllably tune the phase transition temperature of VO_2 materials over a wide range toward practical applications. Furthermore, the rolling-up process is reversible. A VO_2 microtube can be transformed back into a nanomembrane by introducing an external strain. Because of its tunable phase transition temperature and reversible shape transformation, the VO_2 nanomembrane-microtube structure is promising for device applications. As an example application, a tubular microactuator device with low driving energy but large displacement is demonstrated at various triggering temperatures.

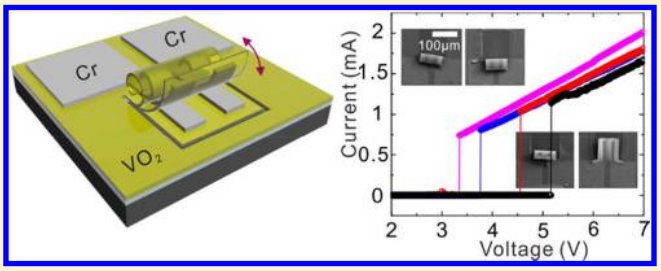

KEYWORDS: *Strain engineering, nanomembranes, vanadium dioxide, actuator, microtubes, phase transition*

Vanadium dioxide (VO_2) displays a profound phase transition between metallic and insulating character, giving it various potential applications in microelectronics and photonics.[1] The electronic, optical, and mechanical properties of VO_2 undergo a dramatic change across the phase transition, which can be used for domain switches,[2] mid-infrared sensors,[3] stress sensors,[4] and artificial muscles.[5] The phase transition of pristine VO_2 materials occurs at approximately 340 K, but the phase transition temperature is strongly influenced by external strain.[6] It was reported that the phase transition temperature decreased almost 50 K (from 341 to 294 K) upon introducing an external compressive strain as small as 1.5%.[7] Although various structural forms in the family of VO_2 materials, such as bulk crystals,[8] thin films,[9] nanowires/nanobeams,[2−4,6] and nanoparticles,[10] have been widely studied, research into strain engineering has been primarily focused on VO_2 nanobeams and thin films. VO_2 nanobeams are useful for fundamental studies, but their scale up for device applications is not practical. VO_2 thin films, though useful for large-scale device fabrication and production, do not have an ideal structural form for strain engineering research and device applications. High-crystalline VO_2 thin films crack when a certain amount of stain is introduced, and the cracking is generally nonreversible, which becomes the main issue in constructing phase transition electrical or optical devices applicable over a broad temperature range.[7,11] VO_2 thin films with the highest crystallinity are epitaxially grown on TiO_2 substrates; however, they always crack across the phase transition during heating or cooling processes.[12,13] One possible approach to maintaining the advantages of VO_2 thin films for large-scale device production while overcoming the cracking problem is to suspend the VO_2 thin film from the substrate underneath to form a free-standing nanomembrane. In this way, the strain can be relaxed therein without cracking the VO_2 nanomembrane.

Here, we demonstrate a feasible process to fabricate VO_2 nanomembranes, to roll a nanomembrane up into a VO_2 microtube, and to reversibly expand the microtube back into a VO_2 nanomembrane. The ultrathin VO_2 nanomembranes are transferrable and reconfigurable as potential building blocks for applications in phase transition electronics, photonics, and mechanics as well as reconstructable to tubular structures with controllable phase transition temperatures. The roll-up fabrication method is developed with the goal to construct

Received: February 3, 2018
Revised: April 4, 2018
Published: April 10, 2018

DOI: 10.1021/acs.nanolett.8b00483
Nano Lett. 2018, 18, 3017−3023

three-dimensional mesostructures through origami of the nanomembrane system toward device applications. The rolled-up microtubes are formed spontaneously through the mechanism of strain relaxation after releasing the prestrained nanomembranes from substrate, resulting in a redistribution of the competitive relationship among the strained layer.[14−16] The rolled-up tubular mesostructure provides a wide range of potential applications, ranging from lab-in-a-tube[17] and on-chip energy storage[18,19] to optical microcavities[20,21] and micro/nanomotors.[22] The requirement of fabricating inorganic[10,14,18] and organic[15,16] membranes on the scale of several to tens of nanometers is vital to the rolling-up process. Only when the membrane reaches such thinness can they be designed in 3D mesostructured[14,23] and flexible devices,[5,24] which are difficult or impossible to fabricate using 0D and 1D nanomaterials. As the outstanding phase transition properties of VO_2 have attracted great attention for microelectronic and optoelectronic devices,[25−27] it would be intriguing to develop devices based on VO_2 nanomembranes. Small-area VO_2 membranes were previously fabricated in a localized region by completely etching away the thick substrate from the backside of the substrate with a standard solid oxide fuel cell (SOFC) process;[28] however, the membrane is not completely suspended or free-standing because the majority of the area of the VO_2 thin film is still closely attached to the substrate (except the backside hole region); hence, the strain therein cannot be fully relaxed. Furthermore, the SOFC-like fabrication process is complicated, time-consuming, and inefficient, and buckling is inevitably introduced to the VO_2 membranes in the fabrication process, which hinders their practical applications for functional devices and large-scale integration.

In this work, the thinning method and self-rolling-up nanotechnology are combined, and a bimorph based on an ultrathin VO_2 nanomembrane is fabricated, which is constructed in microtubular structure due to the low bending stiffness of the bilayer nanomembrane system. The rolled-up tubular structure can incorporate fault-tolerant methodologies[29] because a change in strain in the nanomembrane redistributes the strain inside the bilayer nanomembrane and leads to an additional compressive strain in the outer layer consisting of VO_2, which can be tuned via the deposition thickness of the structural layer. Through such strain engineering, the threshold voltage or temperature to trigger the phase transition can be decreased by controlling the diameter of the tube. Finally, a tubular microactuator with strain compensation, low driving energy, and large displacement is fabricated with different triggering temperatures. Our work provides a new platform to engineer and self-assemble VO_2 nanomembranes with reconfigurable tubular structures for advanced microelectromechanical systems, nanoelectromechanical systems, and micro-opto-electro-mechanical systems.

The schematic of the microfabrication process is illustrated in Figure 1a. First, a 200 nm-thick VO_2 film was deposited by sputtering on a SiO_2(300 nm)/Si substrate. A cross-sectional scanning electron microscopy (SEM) image illustrating the heterostructure stack is shown in Figure 1b. The polycrystalline VO_2 thin film has a columnar structure with an average grain size on the order of ∼100 nm. In the second step, fluorine-based plasma etching was carried out to thin VO_2 to the desired thickness. In the fluorine-based plasma etching method, a reactive gas interacts with the surface through a chemical etching process. Compared with the commonly reported Ar ion beam-based VO_2 drying process,[30] which inevitably imparts

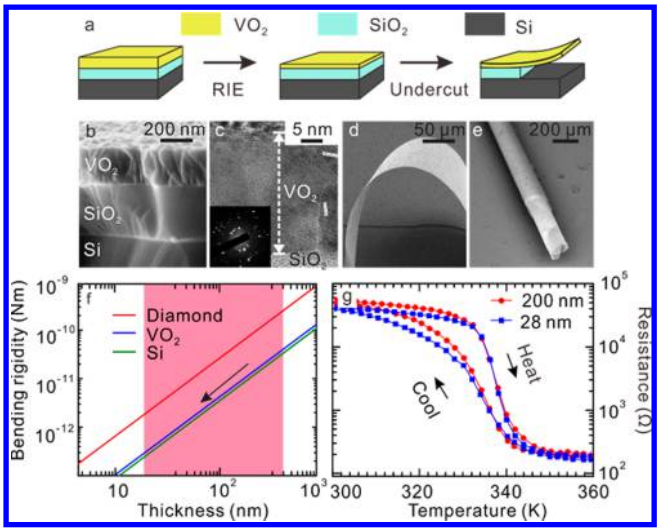

Figure 1. Fabrication and characteristics of an ultrathin VO_2 nanomembrane. (a) Schematic of the microfabrication process using rolling-up nanotechnology. (b) Cross-sectional SEM image of the VO_2 nanomembrane before the thinning process. (c) Cross-sectional TEM image of the thinned VO_2 nanomembrane. (d) SEM image of the ultrathin VO_2 nanomembrane. (e) SEM image of the VO_2 microtube. (f) Bending rigidity of various materials as a function of thickness. (g) Temperature-dependent resistance of VO_2 nanomembranes with thicknesses of 200 and 28 nm. The resistance decreases with increasing temperature and vice versa due to the phase transition.

surface damage to the VO_2 layer due to the physical etching process, the fluorine-based plasma etching method shows negligible damage to the VO_2 layer.[30] The structural and morphological properties of the ultrathin nanomembranes were investigated by cross-sectional transmission electron microscopy (TEM), as shown in Figure 1c. The smooth surface and clear boundary indicate that no surface damage was produced on the VO_2 nanomembrane, which confirms the high quality of the nanomembranes. The polycrystalline nature of the VO_2 layer was observed in the high-resolution TEM image (Figure S1) and further confirmed by selected area electron diffraction (SAED, inset of Figure 1c). In the third step, the VO_2 nanomembrane is released from the substrate by removing the SiO_2 layer using a diluted hydrofluoric acid solution, as shown in Figure 1d. Driven by its intrinsic stress gradient, the free-standing structure bends into a tube, as shown in Figure 1e.

Figure 1f shows the bending rigidity as a function of thickness for three different materials. At the same thickness, the bending rigidity of VO_2 is higher than that of Si but lower than that of diamond,[14] described as a hard material by its high Young's modulus (140 GPa). In our experiment, the thinning of the VO_2 nanomembrane reduces its flexural rigidity (shown as the red area in Figure 1f), which allows the formation of three-dimensional nanostructures. To study the phase transition properties of the VO_2 nanomembrane before and after the reactive ion etching (RIE) process, we measured the resistance as a function of temperature in VO_2 films with different thicknesses, as presented in Figure 1g. Across the phase transition at 340 K, the VO_2 nanomembrane with a thickness of 28 nm exhibits a drastic change in resistivity by over two orders of magnitude, to almost the same level as the thin film. In addition, it is noted that the resistance of VO_2 in the insulating state is slightly lower for the thinner VO_2 membrane compared with the thicker membrane. This decrease

DOI: 10.1021/acs.nanolett.8b00483
Nano Lett. 2018, 18, 3017−3023

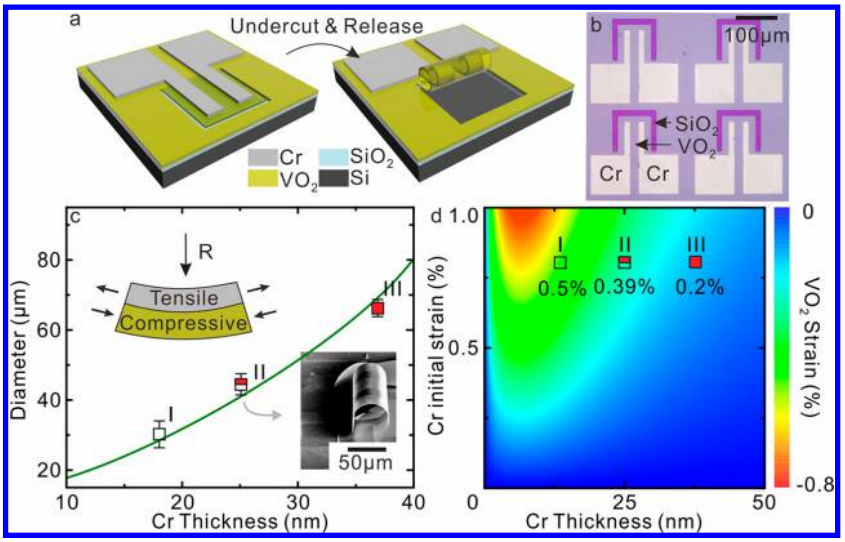

Figure 2. Characteristics of a bimorph based on an ultrathin VO_2 nanomembrane. (a) Schematic of the fabrication of the Cr/VO_2 bimorph structure by selective etching of the SiO_2 sacrificial layer. The strain gradient in the bimorph rolls the nanomembrane into a tubular structure after release. (b) Top view of four devices patterned out of the Cr/VO_2 bimorph. The light purple area is covered by VO_2. The dark purple area is the SiO_2 layer exposed by the selective etching of VO_2. The white area is the patterned Cr layer, which acts as the electrodes. (c) Calculation of the relationship between the diameter of the Cr/VO_2 bimorph and the Cr thickness. The experimental results of tuning the Cr thickness are plotted on the curve (I, II, III) according to the corresponding Cr thickness. The upper inset shows the formation mechanism for the strain-induced self-rolling of the Cr/VO_2 bilayer. The lower inset shows the SEM image of the corresponding sample. (d) Mapping of the bending-induced VO_2 strain related to the thickness of the Cr layer with different initial strains. Spots I, II and III are the same samples as in panel c. The VO_2 strains of I, II and III are calculated to be 0.5%, 0.39%, and 0.2%, respectively.

in resistance is likely attributed to the inhomogeneous oxygen stoichiometry when VO_2 is exposed to O_2 plasma, which introduces defect states in the VO_2 band gap.[31] With increasing temperature, the resistances of both samples drop slowly but do not become equal until the temperature is close to the phase transition temperature. During the phase transition, the electrical conductivity of the VO_2 film in the metallic phase does not show a great decrease after thinning (from 200 to 28 nm), which can be attributed to the formation of a conductive amorphous film of VO_2 with lower resistance on the surface by O-ion bombardment.[32] Hence, the hysteresis curves presented between the cooling and heating processes of both samples indicate that the conduction mechanism does not change between the thick film and the nanomembrane after RIE.

As the bending rigidity can be dramatically decreased by the thinning process, the internal stress gradient can be enhanced with a top stressor to generate sufficient bending energy for a small diameter. Thus, a patterned Cr layer was deposited on the surface of the ultrathin VO_2 nanomembrane to serve as the structural layer. The Cr layer induces an additional strain gradient, permitting the Cr/VO_2 bimorph to roll into a tubular structure and also serves as electrode for testing the electrical properties of the ultrathin VO_2 nanomembrane. Such a two-terminal device, shown schematically in Figure 2a, is composed of two Cr electrodes on the ultrathin VO_2 nanomembrane, where the electrodes are designed with widths of 10 μm separated by a 20 μm gap. Optical images of the patterned devices via two-step RIE before the etching process are shown in Figure 2b. The first RIE process aims to expose the SiO_2 layer to determine the etching direction, while the second RIE process partially etches the VO_2 layer into an ultrathin nanomembrane. Additional details of the fabrication process are discussed in Figure S2.

It is well-known that the layer thickness and strain gradient have a strong influence on the resultant rolling diameter.[33] In our Cr/VO_2 bilayer, rolling always occurs in the upward direction, as shown in the lower inset of Figure 2c. Hence, the strain gradient can be inferred as follows: Cr layer as tensile strain and VO_2 bilayer as compressive layer as shown in upper inset of Figure 2c. The relationship between the final diameter and the thickness of the Cr layer was investigated and is illustrated in Figure 2c. On the basis of the elastic mechanism, the diameter can be calculated from a given internal strain and thickness with the following formula:[33]

$$\frac{1}{Diameter} = \frac{6E_1'E_2't_1t_2(t_1+t_2)(\eta_1\varepsilon_1^{\,0}-\eta_2\varepsilon_2^{\,0})}{(E_1')^2t_1^{\,4}+(E_2')^2t_2^{\,4}+2E_1'E_2't_1t_2(2t_1^{\,2}+2t_2^{\,2}+3t_1t_2)}$$

where $E_i' = E_i/(1-\nu_i^2)$, $\eta_i = 1+\nu_i$ $(i = 1,2)$ for plane strain situation.

Here, $i = 1,2$ refers to the first (VO_2) and second (Cr) layer; E_i and ν_i are the Young's modulus and Poisson's ratio, respectively; t_i is the thickness; and $\varepsilon_i^{\,0}$ is the initial strain in each layer. The result of the calculation is plotted as the green curve in Figure 2c. Upon increasing the Cr layer thickness from 18 to 37 nm, the diameter of the bimorph increases from 30 to 66 μm and can be adjusted down to approximately 7 μm on the basis of the Timoshenko formula.[33] The lower inset of Figure 2c shows the SEM images of the corresponding sample. Additional SEM images of the corresponding samples with different diameters are shown in Figure S3. As reflected by the corresponding data points in Figure 2c, the experimental results are in good agreement with the theoretical curves.

As the Cr/VO_2 bimorph rolls into a tubular structure with a tunable diameter, the strain inside the bimorph is redistributed in the vertical direction. Generally, the outer wall of the tube generates compressive strain, while the inner wall generates tensile stress.[34] The interface between the tensile layer and

DOI: 10.1021/acs.nanolett.8b00483
Nano Lett. 2018, 18, 3017−3023

compressive layer is defined as the neutral plane, where the strain is zero without any deformation.[35] In the Cr/VO_2 bimorph system, the outer VO_2 layer typically suffers from compressive strain, depending on the neutral plane and geometrical deformation. More detail is shown in Figure S4. The influence of the rolling diameter, which is determined by the Cr thickness and the initial strain, on the VO_2 nanomembrane strain redistribution was calculated, as shown in Figure 2d. It is clear that increasing the initial strain results in a small diameter. Meanwhile, the thinner Cr layer reduces the rigidity of the bilayer, also leading to a small diameter. As a consequence, the smaller diameter allows the VO_2 layer to stretch more, reaching a higher compressive strain state. The experimental results shown in Figure 2c are also plotted in Figure 2d according to the corresponding Cr initial strain and thickness. In this way, we evaluated that the changes in the average compressive strain in these three samples (I, II, III) are 0.5%, 0.39%, and 0.2%, respectively. This VO_2 strain redistribution through nanomembrane bending may provide an effective way to tune the VO_2 phase transition temperature.

The phase transition of the fabricated bimorph system was examined by measuring the electrical properties. The change in the electronic structure across the phase transition is accompanied by a several orders of magnitude change in the electrical resistivity of VO_2, which exhibits a conductance switching phenomenon.[36,37] This transition can be triggered by global heating or by Joule heating induced by a current flow. In our experiment, a dielectric thin Al_2O_3 (100 nm) layer was coated on four devices of types I, II, III (shown in Figure 2), and IV (planar bimorph as a reference) using atomic layer deposition (ALD, Figure S5) to fix the strain of the bimorph. Without ALD coating to fix the strain, the $I-V$ characteristics show a slight nonlinear behavior and a high phase transition temperature (Figure S6). The SEM images of these four devices are shown in Figure 3a, which reveal that the bimorph is rolled-up into tubes with different diameters. Thus, the redistributed strain in the VO_2 nanomembrane is different, as depicted in each image in Figure 3a. A voltage is applied through two microprobes that puncture the brittle Al_2O_3 layer and attach to the surface of Cr, and an electric field is established across the gap, allowing a small current through the insulated VO_2 nanomembranes. Figure 3b illustrates the $I-V$ characteristics of the devices with different compressive strains modified by diameter. All devices exhibited the conductance switching phenomenon of a sharp rise in current, reflecting the fast transition of VO_2 from a high resistivity state to a low resistivity state when the voltage was increased above the threshold point (V_{ON}, I_{ON}). Furthermore, V_{ON} monotonically decreased with increasing compressive stain. On the other hand, the corresponding change in V_{ON} implied that the compressive strain was successfully redistributed in the ultrathin VO_2 nanomembrane. The lowest V_{ON} was 3.33 V for the device with 0.5% compressive strain, while the highest V_{ON} was 5.18 V for the strain-free device. A similar conductance switching phenomenon has been reported for a VO_2 nanobeam with a thickness of 500 nm and width of 1 μm^2. By comparing the V_{ON} of the two types of devices, nanobeam and nanotube, our devices showed a lower V_{ON} at the same compressive strain state, implying that a lower energy was required for the phase transition. We attribute this phenomenon mainly to the distribution of Joule heating between parallel Cr electrodes, which is simulated in the inset of Figure 3b. In addition, the

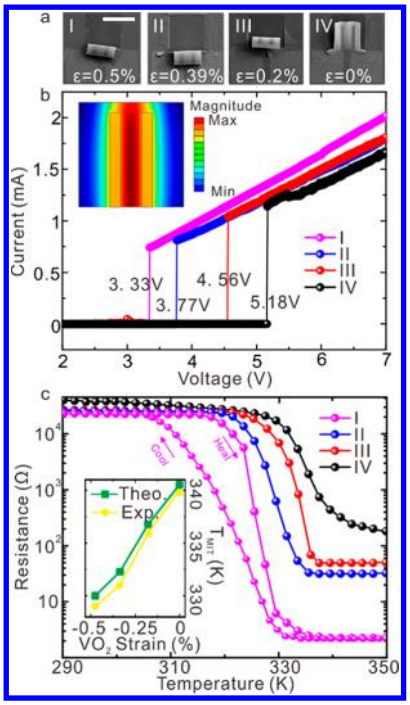

Figure 3. Properties of the Cr/VO_2 bimorph structures, which are responsive to various external stimuli. (a) SEM images of the Cr/VO_2 bimorphs with various diameters. The scale bar is 100 μm. The strain is obtained in accordance with Figure 2. (b) $I-V$ characteristics of the Cr/VO_2 bimorphs under different compressive strains. The inset is the simulated thermal field profile when 0.1 V voltage is applied over a 20 μm gap. The heat aggregated between the electrode leads to a low transition voltage. In addition, the compressive strain lowers the voltage by tuning the phase transition temperature. (c) Resistance of the Cr/VO_2 bimorphs under different compressive strains related to the temperature. The magenta curve shows the heating−cooling cycle, while the curves in other colors show only the heating process. The inset depicts the experimental and calculation results of the phase transition temperature effected by the bending-induced VO_2 strain. The experimental results agree with theory that the phase transition temperature decreases with increasing compressive strain.

ultrathin VO_2 nanomembrane requires less energy to be heated compared with the thicker film or bulk VO_2.

The reduction in the resistivity change of the representative four devices with various strain states was also investigated, and the resistivity versus temperature plot is shown in Figure 3c. Here, instead of heating by electrical current, by which an accurate temperature is hard to obtain, heating by hot plate was applied. At the same time, the resistance of the bimorph was measured by applying a tiny voltage with negligible heating effect. By comparing the resistance data presented in Figure 3b with those in Figure 3c, a large discrepancy can be observed, which could be due to the different fractions of conductive areas in the metal-phase VO_2 films when global heating (baking) and Joule heating are adopted (details are shown in Figure S7). It is noted that the resistances increase with decreasing strain when VO_2 is in the metallic phase, as shown in Figure S8, which is due to the R-O phase transition in different strain states.[38] Our device with 0% compressive strain (black line in Figure 3c) presents a similar curve to the original ultrathin VO_2 nanomembrane (Figure 1g). In addition, the phase transition temperature decreases with increasing redistributed compressive strain in VO_2. This shows that the phase transition temperature can be tuned to 329 K by applying

DOI: 10.1021/acs.nanolett.8b00483
Nano Lett. 2018, 18, 3017−3023

0.5% compressive strain. In the heating process, the resistance of device I starts to deviate from the insulating state at 318 K and reaches a stable, metallic state that is three orders of magnitude lower than that of the insulating state at room temperature. Upon cooling, the resistance gradually increases at 330 K and returns to the original resistance at 308 K. Moreover, the ultrathin VO_2 nanomembrane demonstrates a smaller hysteresis width than the thick film,[39−41] which is useful for high-speed switching devices.[42,43] The heating and cooling cycles of other devices are shown in Figure S9. Furthermore, we compared our experimental results to the VO_2 phase diagram,[7] which shows the VO_2 phase related to the strain and temperature. The comparison is illustrated in the inset of Figure 3c. The experimental results are in good agreement with the phase transition temperature obtained from phase diagram according to the distributed strain. A slight decrease in the measured phase transition temperature is observed in our devices due to the decrease in the phase transition temperature caused by the thinning of the VO_2 nanomembrane.[30,44−46]

As previously mentioned, the bimorph was coated with Al_2O_3 to fix the redistributed strain to obtain an accurate relationship between the phase transition temperature and the VO_2 strain. The phase transition of VO_2 will generate 1−2% compressive strain during the transition from the insulating phase to the metallic phase, which can be applied in actuators driven by heat.[47] Such heating effect can be demonstrated by direct baking (in an oven or on a hot plate) or Joule heating by electrical current.[36,37] We proved that both cases can be applied to our bimorph device, and direct heating was adopted for demonstration. Figure 4a, representing individual captures of Supplementary Movie 1, shows the actuating behavior of the VO_2/Cr bimorph device with temperature change. Initially, the nanomembrane rolls into a tubular structure (red square in Figure 4a) due to the strain gradient generated by the deposited Cr layer. With increasing temperature, VO_2 undergoes a phase transition, leading to additional compressive strain in the outer layer of the tubular structure. Therefore, the diameter increases and the tubular structure collapses to a planar nanomembrane when VO_2 transforms into the metallic phase. Then, the heating stops, and the system starts to cool to room temperature. VO_2 suffers from an opposite transition, so the bimorph rolls into a tubular structure again. The quantitative analysis of the curvature (the reciprocal of the diameter) change as a function of temperature is illustrated in Figure 4b. The tested samples are the same as those in Figure 3a, denoted I, II, III and IV. Each device undergoes a heating−cooling cycle to obtain a hysteresis curve, as illustrated in Figure 4b. The initial curvature of each is different due to the different VO_2 compressive strain redistribution. Each device undergoes a strain change generated from the phase transition, but such nanomembranes can only curve downward slightly because of the limited space underneath the substrate. It is observed that the curvature of the VO_2/Cr bimorph changes by 4.5×10^4 m^{-1} or more, which is much better than existing VO_2 microactuators.[5,39−43,48,49] This large change in curvature is attributed to the low bending stiffness of ultrathin VO_2, which makes the required actuating energy very low. Moreover, for different devices in different strain states, the change in curvature occurs at a different temperature, reflecting the phase transition temperature variation due to compressive strain in VO_2. Also, this temperature shift is in agreement with the previous electrical testing of a fixed bimorph, while the transition point shifts to higher temperature as a result of compressive strain relaxation when the structure is not fixed.

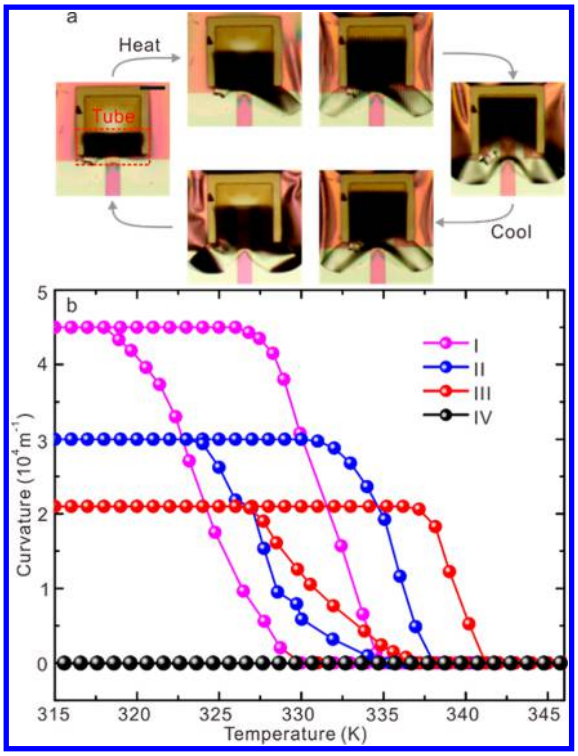

Figure 4. Actuating behavior of the Cr/VO_2 bimorph devices triggered by temperature. (a) Optical images of rotation of the tube at various temperatures in a heating−cooling cycle. The dark part is the bimorph rolling into a tube (red rectangle) at low temperature and flattened into a rectangular nanomembrane. The scale bar is 30 μm. (b) Dependence of the Cr/VO_2 bimorph curvature at various strains on the temperature across the phase transition. The rolled bimorph flattens when the transition temperature is dependent on the compressive strain. The dark line presents no change in curvature because the flat nanomembrane is attached to the substrate.

In conclusion, a free-standing ultrathin VO_2 nanomembrane is fabricated by a thinning process and etching of an underlying sacrificial layer. The self-rolling of the ultrathin VO_2 nanomembrane is achieved via the additional deposition of a strained Cr layer to build a Cr/VO_2 bimorph. As a consequence of the rolling-up of the ultrathin Cr/VO_2 bimorph, the strain inside the bilayer nanomembrane system is redistributed, which leads the outer layer of the ultrathin VO_2 to suffer from additional compressive strain. A theoretical model is put forward to map the redistributed VO_2 strain related to the thickness of the deposited Cr and the initial strain, which indicates the tunability of our rolled-up microtubular structure. The redistributed strain, which can be tuned from 0% to 0.5% by varying the tube diameter, lowers the phase transition temperature from 341 to 329 K, as well as the phase transition threshold voltage. Without fixing the tubular structure, the Cr/VO_2 bimorph can reversibly transform between the rolled-up tubular structure and planar structure by changing the temperature. The driving temperature can also be tuned by tuning the redistributed compressive strain. Benefiting from the low bending stiffness of the ultrathin nanomembrane, this actuator requires low energy to trigger the actuating behavior, and a curvature change of more than 4.5×10^4 m^{-1} is observed in our system. Our work presents new structural forms of VO_2 materials, that is, VO_2 nanomembranes and microtubes, as well

DOI: 10.1021/acs.nanolett.8b00483
Nano Lett. 2018, 18, 3017−3023

as a new platform to study strain engineering in VO_2 materials along with their device applications. A high-performance microactuator device self-assembled from VO_2 nanomembranes is demonstrated.

The proposed concept of free-standing and tubular nanomembranes could create a bridge between material properties and architecture geometry for materials research involving assembly and self-assembly,[14,50] which could allow the application of two-dimensional (2D) concepts to conventional material platforms. The strategy we considered here requires only the lift-off technique and strain engineering for target materials. For example, to adjust the quantum structure, researchers have put great effort into tuning the strain to obtain desirable electronic properties,[51] but the examined host substrates are limited, which could be overcome using nanomembranes.[52] To process conventional materials, their thin-film structure needs to be constructed with lift-off capability, which typically can be achieved with an inserted sacrificial layer and subsequent undercutting by an etchant. Another lift-off method is to use ion implantation and subsequent cutting. With the above methods, most inorganic materials could be constructed with a nanomembrane structure. Under the appropriate strain engineering, such nanomembranes could be expediently assembled or self-assembled into 3D architectures, including tubes, spirals, wrinkles and other origamis,[50,53] which could lead to a new family of material forms with novel properties. Hence, we believe that our demonstration on VO_2 exemplifies our vision of free-standing and tubular nanomembranes for other inorganic materials as well as 2D materials.

■ ASSOCIATED CONTENT

Supporting Information

The Supporting Information is available free of charge on the ACS Publications website at DOI: 10.1021/acs.nanolett.8b00483.

Morphology of thinned VO_2 membranes; fabrication process; morphology of thin VO_2 bimorph nanomembranes; calculation of bending rigidity; Al_2O_3 coating; properties of Cr/VO_2 bimorph structures (PDF)

Movie showing actuating behavior of microactuators triggered by temperature (AVI)

■ AUTHOR INFORMATION

Corresponding Author

*E-mail: yfm@fudan.edu.cn.

ORCID

YongFeng Mei: 0000-0002-3314-6108

Author Contributions

⊥Z.T. and B.X. contributed equally. Y.M. and Z.Y. conceived the concept. L.S. and Z.Y. optimized the VO_2 thin-film growth conditions, and B.H. performed the VO_2 thin-film growth under the supervision of Z.Y. Z.T. and B.X. carried out the fabrication and characterization of the VO_2 nanomembranes and microtubes, Z.T. measured the actuating properties, and Z.T. and B.X. performed the theoretical modeling and numerical simulations under the supervision of Y.M. Z.T., B.X., Z.Y., and Y.M. cowrote the manuscript. All authors discussed the results and commented on the manuscript.

Notes

The authors declare no competing financial interest.

■ ACKNOWLEDGMENTS

This work is supported by the Science and Technology Commission of Shanghai Municipality (No. 17JC1401700), the Natural Science Foundation of China (Nos. 51322201, U1632115, 51602056), and the China Postdoctoral Science Foundation (No. KLH2021039). Part of the experimental work was carried out at the Fudan Nanofabrication Laboratory. Part of the work was performed at the Center for Nanoscale Materials, a U.S. Department of Energy Office of Science User Facility, and supported by the U.S. Department of Energy, Office of Science, under Contract No. DE-AC02-06CH11357. We thank Xin Ou from the Shanghai Institute of Microsystem and Information Technology for assistance with the experiment.

■ REFERENCES

(1) Yang, Z.; Ko, C.; Ramanathan, S. *Annu. Rev. Mater. Res.* **2011**, *41*, 337.

(2) Hu, B.; Zhang, Y.; Chen, W.; Xu, C.; Wang, Z. L. *Adv. Mater.* **2011**, *23*, 3536.

(3) Huber, M. A.; Plankl, M.; Eisele, M.; Marvel, R. E.; Sandner, F.; Korn, T.; Schüller, C.; Haglund, R. F.; Huber, R., Jr.; Cocker, T. L. *Nano Lett.* **2016**, *16*, 1421.

(4) Hu, B.; Ding, Y.; Chen, W.; Kulkarni, D.; Shen, Y.; Tsukruk, V. V.; Wang, Z. L. *Adv. Mater.* **2010**, *22*, 5134.

(5) Liu, K.; Cheng, C.; Suh, J.; Tang-Kong, R.; Fu, D.; Lee, S.; Zhou, J.; Chua, L. O.; Wu, J. *Adv. Mater.* **2014**, *26*, 1746.

(6) Cao, J.; Ertekin, E.; Srinivasan, V.; Fan, W.; Huang, S.; Zheng, H.; Yim, J. W. L.; Khanal, D. R.; Ogletree, D. F.; Grossman, J. C.; Wu, J. *Nat. Nanotechnol.* **2009**, *4*, 732.

(7) Cao, J.; Gu, Y.; Fan, W.; Chen, L. Q.; Ogletree, D. F.; Chen, K.; Tamura, N.; Kunz, M.; Barrett, C.; Seidel, J.; Wu, J. *Nano Lett.* **2010**, *10*, 2667.

(8) Ladd, L. A.; Paul, W. *Solid State Commun.* **1969**, *7*, 425.

(9) Lu, J. W.; West, K. G.; Wolf, S. A. *Appl. Phys. Lett.* **2008**, *93*, 262107.

(10) Donev, E. U.; Lopez, R.; Feldman, L. C.; Haglund, R. F., Jr *Nano Lett.* **2009**, *9*, 702.

(11) Paik, H.; Moyer, J. A.; Spila, T.; Tashman, J. W.; Mundy, J. A.; Freeman, E.; Shukla, N.; Lapano, J. M.; Engel-Herbert, R.; Zander, W.; Schubert, J.; Muller, D. A.; Datta, S.; Schiffer, P.; Schlom, D. G. *Appl. Phys. Lett.* **2015**, *107*, 163101.

(12) Lee, D.; Lee, J.; Song, K.; Xue, F.; Choi, S.; Ma, Y.; Podkaminer, J.; Liu, D.; Liu, S.; Chung, B.; Fan, W.; Cho, S. J.; Zhou, W.; Lee, J.; Chen, L.; Oh, S. H.; Ma, Z.; Eom, C. *Nano Lett.* **2017**, *17*, 5614.

(13) Fan, L. L.; Chen, S.; Luo, Z. L.; Liu, Q. H.; Wu, Y. F.; Song, L.; Ji, D. X.; Wang, P.; Chu, W. S.; Gao, C.; Zou, C. W.; Wu, Z. Y. *Nano Lett.* **2014**, *14*, 4036.

(14) Rogers, J. A.; Lagally, M. G.; Nuzzo, R. G. *Nature* **2011**, *477*, 45.

(15) Ionov, L. *Polym. Rev.* **2013**, *53*, 92.

(16) Ionov, L. *J. Mater. Chem.* **2012**, *22*, 19366.

(17) Mei, Y. F.; Huang, G.; Solovev, A. A.; Ureña, E. B.; Mönch, I.; Ding, F.; Reindl, T.; Fu, R. K. Y.; Chu, P. K.; Schmidt, O. G. *Adv. Mater.* **2008**, *20*, 4085.

(18) Huang, W.; Yu, X.; Froeter, P.; Xu, R.; Ferreira, P.; Li, X. *Nano Lett.* **2012**, *12*, 6283.

(19) Bof Bufon, C. C.; Cojal González, J. D.; Thurmer, D. J.; Grimm, D.; Bauer, M.; Schmidt, O. G. *Nano Lett.* **2010**, *10*, 2506.

(20) Wang, J.; Zhan, T.; Huang, G.; Cui, X.; Hu, X.; Mei, Y. F. *Opt. Express* **2012**, *20*, 18555.

(21) Tian, Z.; Zhang, L.; Fang, Y.; Xu, B.; Tang, S.; Hu, N.; An, Z.; Mei, Y. F.; Chen, Z. *Adv. Mater.* **2017**, *29*, 1604572.

(22) Solovev, A. A.; Mei, Y. F.; Bermúdez Urena, E.; Huang, G.; Schmidt, O. G. *Small* **2009**, *5*, 1688.

DOI: 10.1021/acs.nanolett.8b00483
Nano Lett. 2018, 18, 3017−3023

(23) Fairchild, B. A.; Olivero, P.; Rubanov, S.; Greentree, A. D.; Waldermann, F.; Taylor, R. A.; Walmsley, I.; Smith, J. M.; Huntington, S.; Gibson, B. C.; Jamieson, D. N.; Prawer, S. *Adv. Mater.* **2008**, *20*, 4793.
(24) Zhang, P.; Zhu, F.; Wang, F.; Wang, J.; Dong, R.; Zhuang, X.; Schmidt, O. G.; Feng, X. *Adv. Mater.* **2017**, *29*, 1604491.
(25) Lee, S.; Hippalgaonkar, K.; Yang, F.; Hong, J.; Suh, C. K.; Liu, K.; Wang, K.; Urban, J. J.; Zhang, X.; Dames, C.; Hartnoll, S. A.; Delaire, O.; Wu, J.; et al. *Science* **2017**, *355*, 371.
(26) Kumar, S.; Pickett, M. D.; Strachan, J. P.; Gibson, G.; Nishi, Y.; Williams, R. S. *Adv. Mater.* **2013**, *25*, 6128.
(27) Zhu, Z.; Evans, P. G.; Haglund, R. F., Jr; Valentine, J. G. *Nano Lett.* **2017**, *17*, 4881.
(28) Sim, J. S.; Zhou, Y.; Ramanathan, S. *Nanoscale* **2012**, *4*, 7056.
(29) Ji, H.; Wu, X.; Fan, L.; Krien, C.; Fiering, I.; Guo, Y.; Mei, Y. F.; Schmidt, O. G. *Adv. Mater.* **2010**, *22*, 4591.
(30) Fadlelmula, M. M.; Sürmeli, E. C.; Ramezani, M.; Kasırga, T. S. *Nano Lett.* **2017**, *17*, 1762.
(31) Parker, J. C. *Phys. Rev. B: Condens. Matter Mater. Phys.* **1990**, *42*, 3164.
(32) Sim, J. S.; Zhou, Y.; Ramanathan, S. *Nanoscale* **2012**, *4*, 7056.
(33) Nikishkov, G. P. *J. Appl. Phys.* **2003**, *94*, 5333.
(34) Songmuang, R.; Deneke, C.; Schmidt, O. G. *Appl. Phys. Lett.* **2006**, *89*, 223109.
(35) Zang, J.; Liu, F. *Appl. Phys. Lett.* **2008**, *92*, 21905.
(36) Lee, J.; Lee, D.; Cho, S. J.; Seo, J.-H.; Liu, D.; Eom, C.-B.; Ma, Z. *Appl. Phys. Lett.* **2017**, *111*, 063110.
(37) Lee, J.; Lee, D.; Cho, S. J.; Seo, J.-H.; Liu, D.; Eom, C.-B.; Ma, Z. *Appl. Phys. Express* **2017**, *10*, 091101.
(38) Chen, Y.; Zhang, S.; Ke, F.; Ko, C.; Lee, S.; Liu, K.; Chen, B.; Ager, J. W.; Jeanloz, R.; Eyert, V.; Wu, J. *Nano Lett.* **2017**, *17*, 2512.
(39) Rúa, A.; Cabrera, R.; Coy, H.; Merced, E.; Sepúlveda, N.; Fernández, F. E. *J. Appl. Phys.* **2012**, *111*, 104502.
(40) Dong, K.; Lou, S.; Choe, H. S.; Liu, K.; You, Z.; Yao, J.; Wu, J. *Appl. Phys. Lett.* **2016**, *109*, 023504.
(41) Ma, H.; Hou, J.; Wang, X.; Zhang, J.; Yuan, Z.; Xiao, L.; Wei, Y.; Fan, S.; Jiang, K.; Liu, K. *Nano Lett.* **2017**, *17*, 421.
(42) Wang, K.; Cheng, C.; Cardona, E.; Guan, J.; Liu, K.; Wu, J. *ACS Nano* **2013**, *7*, 2266.
(43) Rúa, A.; Fernández, F. E.; Sepúlveda, N. *J. Appl. Phys.* **2010**, *107*, 074506.
(44) Yang, Z.; Ramanathan, S. *Appl. Phys. Lett.* **2011**, *98*, 192113.
(45) Ham, Y.; Efremov, A.; Min, N.; Lee, H. W.; Yun, S. J.; Kwon, K. *Jpn. J. Appl. Phys.* **2009**, *48*, 08HD04.
(46) Yamin, T.; Wissberg, S.; Cohen, H.; Cohen-Taguri, G.; Sharoni, A. *ACS Appl. Mater. Interfaces* **2016**, *8*, 14863.
(47) Marezio, M.; McWhan, D. B.; Remeika, J. P.; Dernier, P. D. *Phys. Rev. B* **1972**, *5*, 2541.
(48) Cabrera, R.; Merced, E.; Sepúlveda, N.; Fernández, F. E. *J. Appl. Phys.* **2011**, *110*, 094510.
(49) Liu, K.; Cheng, C.; Cheng, Z.; Wang, K.; Ramesh, R.; Wu, J. *Nano Lett.* **2012**, *12*, 6302.
(50) Huang, G. S.; Mei, Y. F. *Adv. Mater.* **2012**, *24*, 2517.
(51) Jovanovi, V.; Biasotto, C.; Nanver, L. K.; Moers, J.; Grtzmacher, D.; Gerharz, J.; Mussler, G.; van der Cingel, J.; Zhang, J. J.; Bauer, G.; Schmidt, O. G. L.; Miglio. *IEEE Electron Device Lett.* **2010**, *31*, 1083.
(52) Sánchez-Pérez, J. R.; Boztug, C.; Chen, F.; Sudradjat, F. F.; Paskiewicz, D. M.; Jacobson, R. B.; Lagally, M. G.; Paiella, R. *Proc. Natl. Acad. Sci. U. S. A.* **2011**, *108*, 18893.
(53) Zhang, Y.; Zhang, F.; Yan, Z.; Ma, Q.; Li, X.; Huang, Y.; Rogers, J. A. *Nat. Rev. Mater.* **2017**, *2*, 17019.

DOI: 10.1021/acs.nanolett.8b00483
Nano Lett. 2018, 18, 3017−3023